Laboratori Nazionali di Frascati

Submitted to Astrophysics Journal

LNF-92/052(P)
10 Giugno 1992

R.L. Golden, C. Grimani, B.L. Kimbell, S.A. Stephens, S.J. Stochaj, W.R. Webber, G. Basini, F. Bongiorno, F. Massimo Brancaccio, M. Ricci, J.F. Ormes, E.S. Seo, R.E. Streitmatter, P. Papini, P. Spillantini, M.T. Brunetti, A. Codino, M. Menichelli, I. Salvatori, M.P. De Pascale, A. Morselli, P. Picozza:

OBSERVATIONS OF COSMIC RAY ELECTRONS AND POSITRONS USING AN IMAGING CALORIMETER

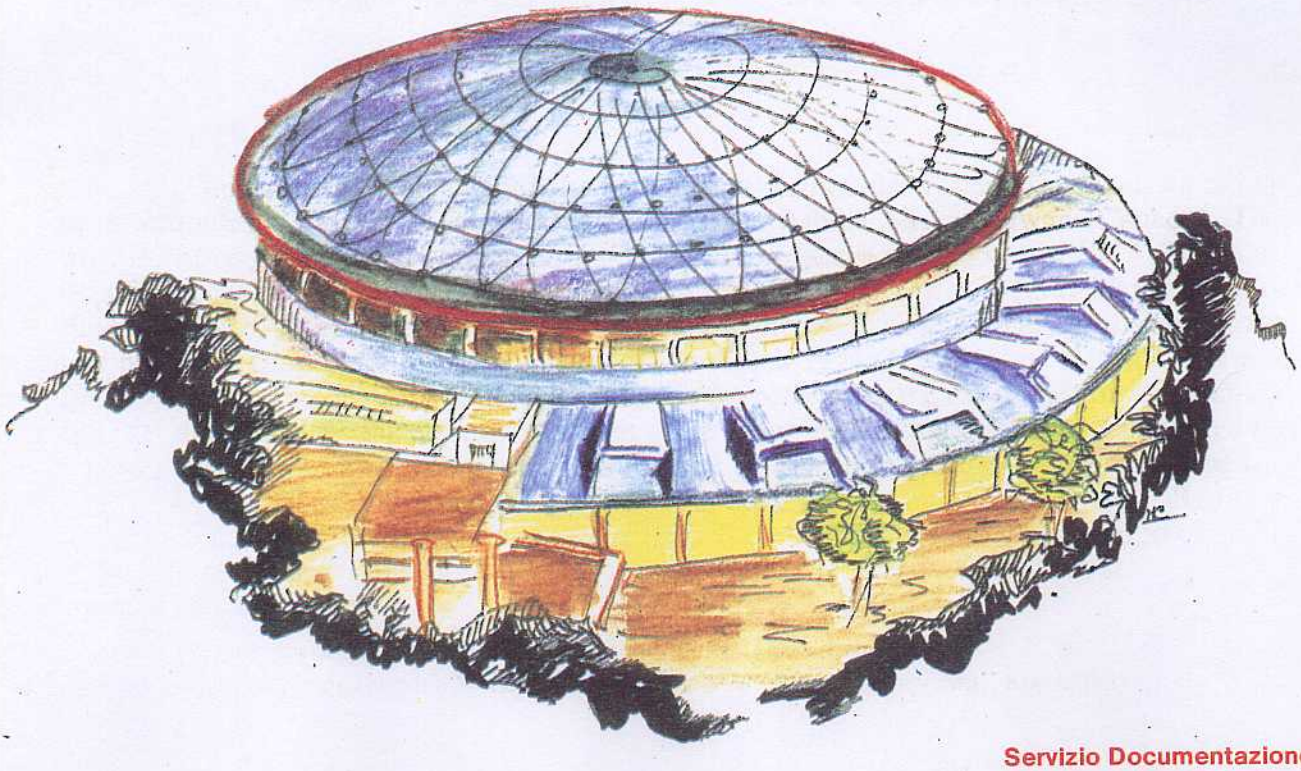

Servizio Documentazione
dei Laboratori Nazionali di Frascati
P.O. Box, 13 - 00044 Frascati (Italy)

INFN – Laboratori Nazionali di Frascati
Servizio Documentazione

LNF-92/052(P)
10 Giugno 1992

OBSERVATIONS OF COSMIC RAY ELECTRONS AND POSITRONS USING AN IMAGING CALORIMETER

R.L. Golden, C. Grimani, B.L. Kimbell,
S.A. Stephens*, S.J. Stochaj, W.R. Webber
New Mexico State University, Las Cruces, NM (USA)

G. Basini, F. Bongiorno**, F. Massimo Brancaccio, M. Ricci
Laboratori Nazionali INFN, Frascati, (Italy)

J.F. Ormes, E.S. Seo
R.E. Streitmatter
NASA/Goddard Space Flight Center, Greenbelt, MD (USA)

P. Papini, P. Spillantini
Dipartimento di fisica dell'Universitá and INFN, Firenze, (Italy)

M.T. Brunetti, A. Codino,
M. Menichelli, I. Salvatori
Dipartimento di fisica dell'Universitá and INFN, Perugia, (Italy)

M.P. De Pascale, A. Morselli, P. Picozza
Dipartimento di fisica dell'Universitá and INFN Sezione di Roma, Tor Vergata, Roma, (Italy)

ABSTRACT

On September 5, 1989 a ballon–borne magnet spectrometer system was flown for 5.5 hr at an altitude of more than 117,000 ft from Prince Albert, Saskatchewan (Canada). The instrument was a modified version of the one used to observe antiprotons in 1979. The most significant modification was the addition of an imaging calorimeter, 7.33 radiation lenghts thick. Inclusion of the calorimeter has significantly improved the ability to distinguish electrons and positrons from the other constituents of the cosmic rays. The absolute electron flux has been determined in the energy interval 1.3–26 GeV (corrected to the top of the atmosphere). At energies above 4 GeV, the electron spectrum at the top of the atmosphere can be represented by a power–law spectrum with constant spectral index. The electron spectrum was found to be $J_{e^-} = 177 \cdot E^{-(3.15 \pm 0.13)}$ electrons/m^2–sr–s–GeV in the energy range 4.0 – 26 GeV. Below 4 GeV the spectrum showed significant flattening. The $e^+/(e^+ + e^-)$ ratio was found to be (0.11 $\pm$ 0.03) in the energy range 5.2 – 13 GeV.

---

* Also Tata Insitute of Fundamental Research, Homi Bhabha Road, Bombay, India

** Also Dipartimento di Metodi e Modelli Matematici dell'Universitá "La Sapienza", Roma, Italy

1. - INTRODUCTION

In this paper we present the first observations of cosmic ray electrons and positrons made using an imaging calorimeter, operated in conjunction with a magnetic spectrometer. Cosmic ray electrons and positrons are of special interest. They are the lowest mass constituent of the cosmic ray charged–particles. Because of their low mass, these particles can lose significant amounts of energy through interactions with the electromagnetic fields as they propagate in the interstellar medium. Measurements of the energy spectra of these particles and comparison of these spectra with those of other species of cosmic rays can give insight into the conditions in the interstellar medium. Some of the data available on electrons has been gathered without the benefit of direct determination of the sign of the particle's charge (see for example Tang, 1984, and Nishimura et al. 1985). Other observations have been based on direct determination of the sign of the particles charge by use of magnet spectrometers (Golden et al. 1984; Buffington et al. 1975). Positron abservations are especially difficult and only a few observations have been made above 1 GeV by magnet spectrometers (Fanselow et al. 1969; Buffington et al. 1975; Golden et al. 1987) and by using the geomagnetic field (Daniel and Stephens 1967; Agrinier et al. 1969; Muller and Tang 1987). Except for the measurements of Buffington et al. (1975), the previous positron observations involve the subtraction of significant backgrounds due to the much larger flux of protons. Measurements at energies above 20 GeV seem to indicate a rise in the $e^+/(e^+ + e^-)$ ratio. This rise could be due to some unanticipated source of energetic positrons or it could simply be the consequence of the ever increasing instrumental difficulty of separating positrons from protons at high energies.

The instrument used for the observations reported here is a modified version of the one used to observe antiprotons in 1979 (Golden et al. 1979). The new configuration incorporates a momentum spectrometer operated in conjunction with a gas Cherenkov detector and the imaging calorimeter. In its present form, the instrument is capable of the unambiguous identification of electrons and positrons over a large energy range. Future flights of the instrument are planned in which the energy range is increased by the substitution of a transition radiation counter (TRD) in lieu of the Cherenkov detector. This will extend the range of unambiguous e^+ identification to well over 50 GeV. The present and future flights in this program are being performed by an international collaboration. The project is commonly refered to as the Matter–Antimatter Spectrometer System (MASS) research program.

There are two difficulties in discussing particle energies in this paper. First, the kinematic quantity determined by the magnet–spectrometer system is magnetic rigidity (momentum/charge) which we express in units of GV/c. The conversion of this quantity to kinetic energy depends on the particle's mass. For fully relativistic singly charged particles the kinetic energy (in GeV) is numerically equal to the rigidity (in GV/c). This is always the case for electrons and positrons in the energy range covered in this paper. But one must be careful when dealing with protons at lower energies. In the following discussions, care has been taken to explicity refer to rigidities (in GV/c) whenever refering to information which has been determined directly from the magnet spectrometer. Otherwise it seems more appropriate refer to a particle's energy. When energies are mentioned, the appropriate kinematic conversions have been made and the

resulting quantities are kinetic energies measured in GeV. The second difficulty is that electrons and positrons loose energy as they propagate through the atmosphere. Thus, for these particles, the energy changes with location. Quantities measured at the spectrometer will always be given in units of rigidity (GV/c). Another location that is sometimes referenced, is at the top of the payload. These energies are derived from the measured rigidities at the spectrometer by correcting for bremstrahlung energy losses associated with traversing the material above the spectrometer in the payload. Finally, for purposes of comparing our observations to others, it is useful to correct the spectra for energy losses both in the payload and in the atmosphere above the payload. Where appropriate, these energies will be denoted by (TOA) which stands for "top of the atmosphere".

The data presented here were gathered on a balloon flight from Prince Albert, Saskatchewan on September 5, 1989. The instrument floated for 5.5 hr at altitudes between 117,000 and 118,500 ft. A preliminary data analysis of this experiment was reported earlier (Basini et al. 1991) and this paper gives the final results. A reflight of this instrument for a longer duration took place in September 1991.

2. - THE APPARATUS

Figure 1 shows the instrument. Signal from Cherenkov detector and all scintillators (T1, T2, S1, T3, T4,) were pulse–height analyzed. The Gas Cherenkov detector was filled with a 50–50 mixture of Freon–12 and Freon–22 giving it a threshold Lorentz factor $\gamma = 23$. Details of the Cherenkov detector performance are given in Golden et al. (1992). The magnet spectrometer consists of 8 high–resolution multi–wire proportional counters (MWPC). All 8 MWPC were measured in the x–axis (the view that has the most curvature). Four MWPC were also digitized in the orthogonal (y–axis) view. Delay–line readouts were used on the MWPC. The arrival times of the MWPC pulses were measured at each end of the delay lines. The sum of each delay line's readout–times was required to be equal to the total propagation time of the line. The magnet was operated at a current of 120 A, producing a magnetic field of 10–40 kilogauss in the MWPC region. The maximum detectable magnetic rigidity (momentum/charge) was 118 GV/c. Details of the magnet spectrometer and its performance are contained in Golden et al. (1991). The calorimeter consisted of 40 layers (20 in each of two orthogonal views) of 64 brass streamer tubes, for a total of 7.33 radiation lengths. The calorimeter also represents 0.75 nuclear interaction lengths of material. Figure 2 shows calorimeter images for four different types of events. As one cas see, the images for different interactions are quite distinct. Since the image data is gathred in digital form, algorithms can be applied directly to the data in order to perform non–subjective tests.

The trigger for an event was a coincidence between T1, T2, T3, and T4. The S1 was then tested by the on–board computer to assure that the pulse–height was greater than 0.25 I_0 (where I_0 corresponds to the pulse–height of a single minimum ionizing particle). Events surviving this test were transmitted to the ground.

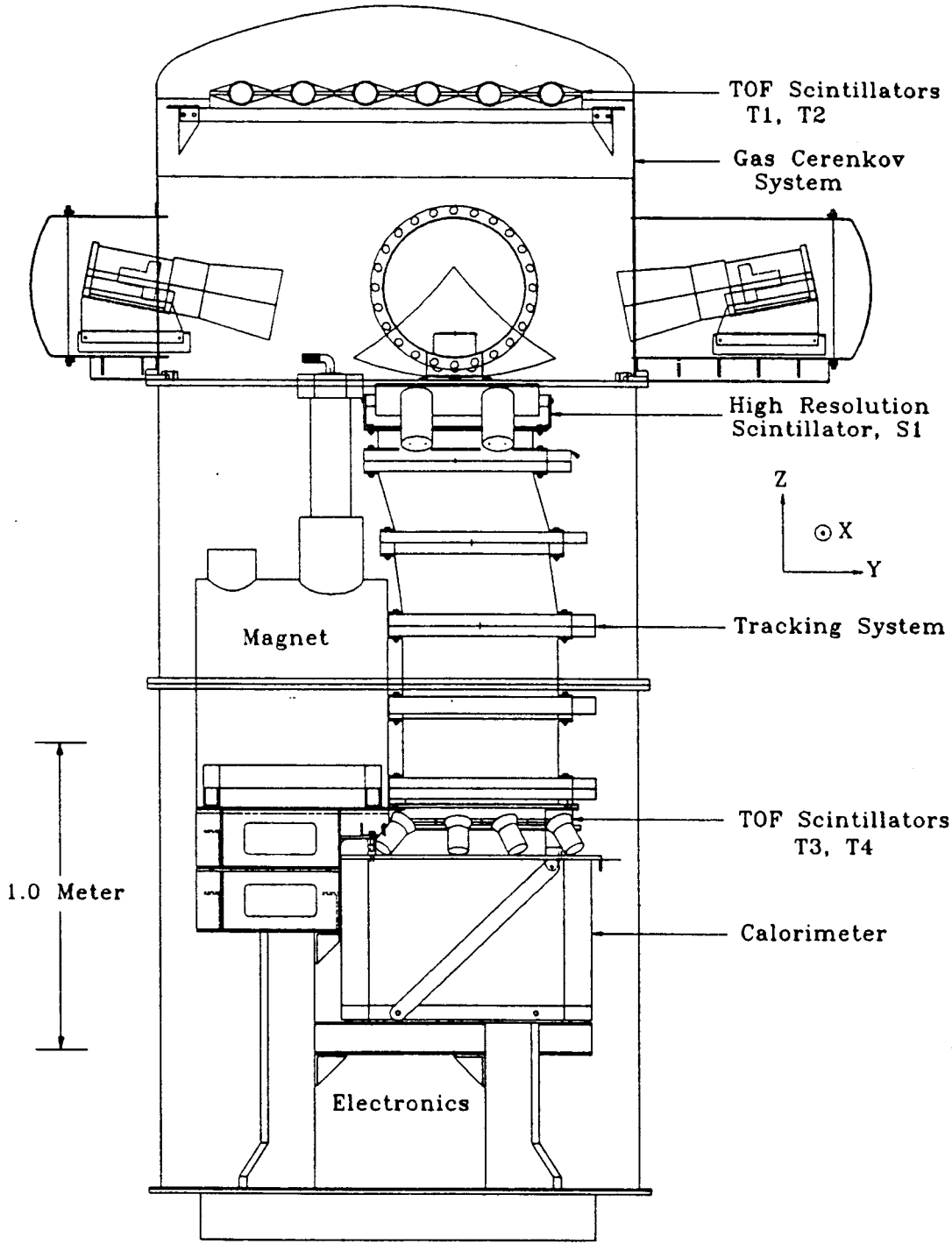

FIG. 1. A schematic diagram of the MASS Instrument.

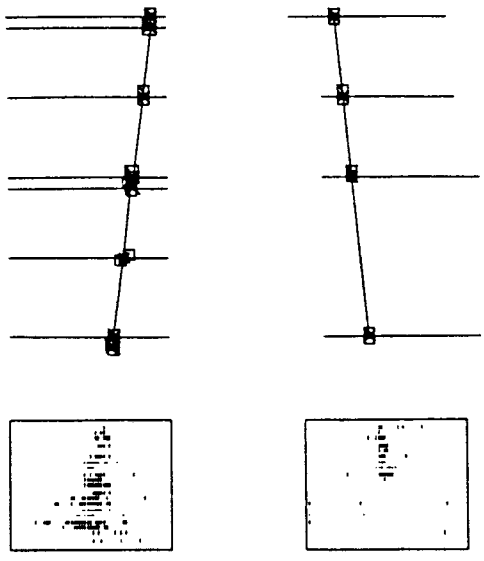

Fig. 2a. A 7GeV electron

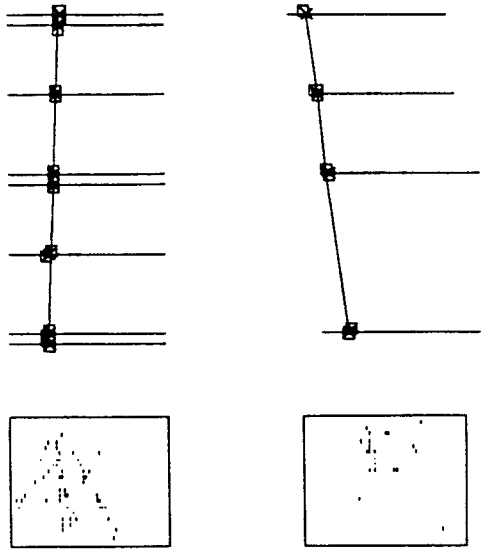

Fig. 2b. A 7GeV proton

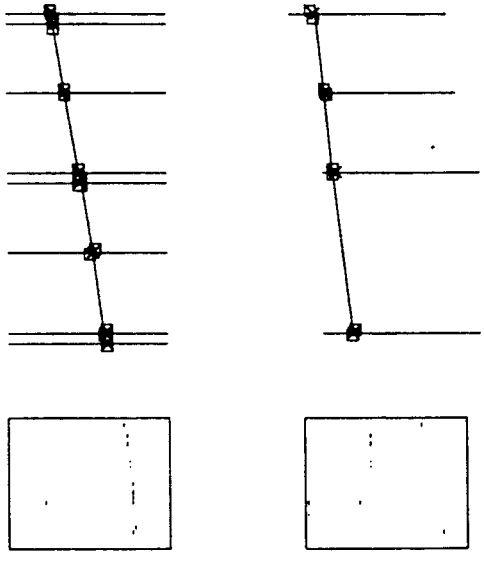

Fig. 2c. A 7GeV muon

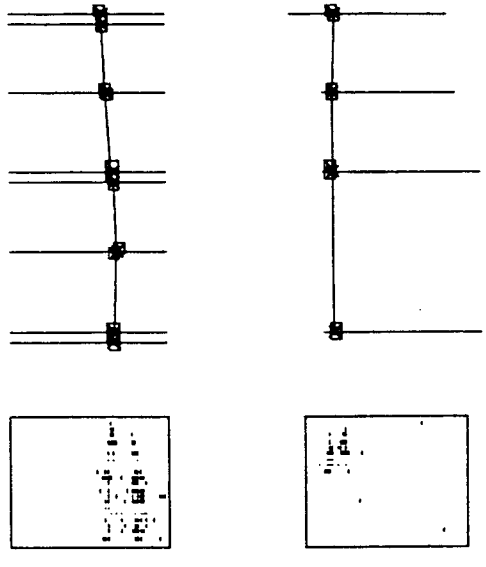

Fig. 2d. A 1.7GeV double-cascade

FIG. 2. Images for 4 different types of events. Each figure shows the MWPC data and the calorimeter image. The left side of each view is the x–view where most of the bending takes place. The right half is the y–view. Note that the lower half of the y–view of the calorimeter was not operating during the flight.

3. – DATA ANALYSIS

a) Selection of e^-

Negatively charged cosmic rays at balloon altitudes are predominantly μ^-, e^- and $\bar{p}$. Pions and kaons will have decayed before reaching the payload because secondary cosmic rays are produced, on the average, 1 scale height (about 7km) above the payload. The negative charge is established using the magnet spectrometer data. Responses of the Cherenkov detector

and calorimeter are used to distinguish e^- from the other negatively charged species. The selection criteria for recognizing e^- consists of 5 tests. The tests used are given in Table I.

TABLE I – Selection Criteria.

Test. 1. At least 5 x–axis and 3 y–axis measurements have good time sums. In addition, certain combinations of "missing" chambers are not allowed. For example, events where both top chambers are "missing" are rejected. This is to assure that the sign of curvature has been measured with high reliability.
Test 2. The least–squares fit to the reconstructed track must have $\chi_x^2 < 5$ and $\chi_y^2 < 7.5$.
Test 3. $\lvert Z \rvert < 1.8\ I_0$
Test 4. Cherenkov pulse–height >= 1 photo–electron.
Test 5. (for electrons) 1.0–2.5 GV/c, no calorimeter requirement 2.5–4.0 GV/c, at least two planes show shower–clusters 4.0–20.0 GV/c, at least five planes show shower–clusters
Test 5. (for positrons). At least 10 planes show shower–clusters.

Test 1 and 2 impose criteria related to the MWPC data and to the associated least squares fit. These tests assure that a negatively charged particle of known energy has been identified. The absolute charge of the particle was determined by scintillators T1, T2, S1, T3. Test 3 eliminates multiple particle events. Muons are an important source of background for e^- observations. Since electrons capable of traversing the spectrometer should all be above the Cherenkov threshold, we required that the Cherenkov detector registers the equivalent of at least 1 photo–electron. The average number of photo–electrons for a fully relativistic particle is about 10. The μ^- Cherenkov threshold rigidity is 2.4 GV/c and the $\bar{p}$ threshold is 22 GV/c. Test 4 eliminates μ^- below 2.4 GV/c and the $\bar{p}$ are eliminated below 22 GV/c.

None of the events selected with Test 1–4 showed interactions with wide angle secondary or starting points below the first few layers in the calorimeter. Either of these characteristics would be indicative of the presence of hadrons. Instead, the remaining events fall into two distinct categories (at rigidities above a few GV/c): 1) a cascade is present, or, 2) no cascade present. Below 20 GV/c the only expected background of significance is due to μ^-. The μ^- produce only a single straight track in the calorimeter. Electrons, on the other hand, produce electromagnetic showers. The lateral spread of these showers is about two Moliere radii (2 x 1.6 cm). Shower recognition was quantified by counting the number of planes in which multiple adjacent wires were triggered within 5 wires of the trajectory extrapolated from the MWPC measurements. Such multiple–adjacent–hits will be refered to as "shower clusters", or simply "clusters". Rigidity dependent selection criteria were used because the background and shower development are rigidity dependent. These criteria are shown in Table I as Test 5 (for

electrons). Over the rigidity range 1 – 2.5 GV/c the efficiency for detecting shower–clusters in the calorimeter is low. While muon and electron tracks can be seen, there are also a large number of events for which no tracks were detected. Therefore, in this rigidity range the Cherenkov counter must be used as the primary instrument for separating muons and electrons. When the histogram of the Cherenkov response for electrons in the 1 – 2.5 GV/c range is compared to electron in the 2.5 – 20 GV/c range, an excess of events with low Cherenkov signal can be seen. We have found that some of these events produce tracks in the calorimeter which are consistent with μ^- like tracks and we assume that they are muons with rigidities just over the Cherenkov threshold. Based on these observations, the muon contamination contributes 10% of events in the rigidity interval 1.0 – 2.5 GV/c.

At rigidities above 2.5 GV/c virtually all electrons produce cascades passing Test 5. Muons at these energies will not pass the cascade tests (due to their inability to produce cascades). Thus muon contamination above 2.5 GV/c is negligible.

b) Selection of e^+

Selection of positrons is more difficult than electrons. This is because the principal component of positively charged cosmic rays (protons) is about 1000 times more abundant than the positrons. Below rigidities of 20 GV/c, particles accompained by Cherenkov light must be e^+, μ^+, or protons accompanied by a "false" Cherenkov pulse (due to photo–tube noise or other non–Cherenkov sources). Golden et al (1992), have shown that the fraction of events below threshold giving a Cherenkov light pulse > 1.0 p.e. is less than 5×10^{-4}. Examination of events accompanied by a Cherenkov pulse shows that many of those with a rigidity above 15 GV/c are accompanied by hadronic cascades. This is due to the MWPC measurement uncertainties that can cause protons with rigidities slightly above 20 GV/c to have fitted rigidities slightly below 20 GV/c. We have limited the upper limit of our observation to 10 GV/c to assure the absence of "spillover" protons.

In the rigidity region 3–10 GV/c, the calorimeter images for positive particles fall into three distinct categories: 1) tightly collimated cascades beginning in the top layers of the calorimeter, 2) wide angle, low multiplicity interactions starting at all depths in the calorimeter, and 3) events with no apparent interaction. Samples of e^- cascades (gathered as outlined above) and protons (identified as positively charged particles between 3 and 10 GV/c not accompanied by a Cherenkov pulse) were studied to develop a quantitative criterion for clearly separating electromagnetic cascades from hadronic cascades. The resulting criteria used for positron identification were the same as 1–5 for electrons except Test 5–(for positrons) is modified to improve the background rejection at the expense of detection efficiency.

The positron version of Test 5 is satisfied by just 59% of e^- in the interval 3–4 GV/c and by 84% of the e^- in the interval 4–10 GV/c. An inspection of the positron candidates passing these criteria reveals that all of the events showed cascades that started in the top 3 layers of the calorimeter. Inspection of e^- cascades below 3 GV/c shows that an increasing percentage of

them fail Test 5 (due to low efficiency in the calorimeter and low multiplicity of the cascades) as the rigidity is decreased. Thus we place a lower limit of 3 GV/c for the observation.

4 - RESULTS

In order to convert the observed counts into an absolute flux one must take into account the geometric factor, exposure time and various selection efficiencies.

The geometric factor was determined by using reconstructed trajectories to determine the horizontal extents of the detectors. The vertical location of each detector was determined by direct mechanical measurement. The resulting detector measurements were used in a Monte Carlo calculation to determine the overall geometric factor. It was found to be 80 cm^2–sr. This is substantially smaller than that used in previous flights of this instrument. The additional height associated with the inclusion of the calorimeter is responsible for most of the reduction. In addition, the outer 5 cm perimeter of the calorimeter area was not used. Restricting the calorimeter geometry assured that calorimeter showers were fully visible.

When each event is encoded, its time of occurence is included in the data package. The total elapsed time is simply the difference between the time of the last event and the first event in the data base. This time was 19,812 seconds. A portion of the observing time is lost due to the time taken to encode and read the data from the digitizing modules. A cumulative clock is started at the beginning of each radout cycle and stopped when readout is complete. The ratio of this "dead time" clock to the total elapsed time is used to determine the fraction of time lost during the readout process. The ratio was checked throughout the flight to verify that the data gathering efficency was not time dependant. The fraction of live time was found to be 0.67 throughout the flight. A large buffer is used to compensate for stochastic fluctuations in the trigger rate that exceed the telemetry transmission rate. The data recording is done by transcription of analog tapes after the flight. A fraction of the events is lost due to the disk–write time of the ground computer system. The disk write time exceeds the buffering capability of the input interface. Each event transmitted by the payload is given a sequential event number. The fraction of events surviving the recording is determined by measuring the fraction of event numbers present in the recorded data. The fraction of events surviving the recording process is 0.94.

The tracking system efficiency is discussed in detail in Golden et al. (1991). The efficiency for passing Test 1 was found to be 0.68 ± 0.05. There is a concern that albedo from the electromagnetic cascades might represent an additional loss. In order to evaluate this additional inefficiency, the maximum opening angle distribution of the e^- cscades was measured. A series of Monte Carlo simulations was performed simulating an ensemble of cascades and histogramming their maximum angle distributions. The critical energy of the target material was adjusted until the simulated angular distribution matched the observed distribution. The critical energy was found to be 25 MeV. Cascades generated with this critical energy were found to have negligible albedo losses. This was confirmed by relaxing the tracking criteria so that many of the hypothetical albedo events could be accepted. No electron cascades

accompanied with albedo have been observed. In contrast, hadronic cascades have been obeserved where the bottom two chambers have multiple track signatures.

The absolute charge test (Test 3) was checked by using events chosen to have $|Z|=1$ in T4. Some events can be expected to fail due to the Landau effect and instrumental resolution. The efficiency for passing this test was found to be 0.96.

We have found that the scintillators used for generating the trigger have a position dependent response. This results in an efficiency of 0.90 in the event trigger.

We have also considered the event loss due to pair production in the payload above the spectrometer. As an electron traverses the payload, it passes through 0.14 radiation lenghts of material before it raches the tracking system. We have calculated the mean photon emission probability for electrons in our energy range and determined the probability of these photons producing e^+, e^- pairs as they propagate through the payload. Pair production causes multiparticle events in the tracking system for which the rigidity can not be determined. The estimated efficiency for events not having "early" pair production is 0.93.

As mentioned earlier, the efficiency for e^- passing the e^- version of Test 5 is regarded to be 1.0. On the other hand, the efficiency for e^+ passing the e^+ version of Test 5 is significantly smaller. This efficiency was measured by applying the e^+ version of Test 5 to the e^-. The efficiency for e^- surviving the e^+ cascade criterion is found to be 0.59 in the range 3 – 4 GV/c and 0.84 in the rigidity range 4 –10 GV/c.

Measuremens of the exposure time and recording efficiency are quite precise. However measurement of selection efficiencies is subject to statistical uncertainties and systematic errors. Many of the measurements rely on selection of species using independent selection techniques and then measuring the efficencies for the species to pass the criterion in question. Experience gained with changing selection criteria and observing changes in the measured efficiencies gives a feeling for the size of the systematic errors. In general, uncertainties comparable to the statistical uncertainties were encountered. To be conservative we estimate that the unceraintly on our overall exposure factor is 20% above 2.5 GV/c. Below 2.5 GV/c the background incrases and the efficiency decreases. The net result is an increase in the uncertainty in the exposure factor to a value of 25%. Note however, uncertainty in the exposure factor will not apply to the $e^+/(e^+ + e^-)$ ratio. The accuracy in $e^+(e^+ + e^-)$ is limited only by statistics.

a) electron results:

Table II contains a summary of the e^- observations. The mean energies at the top of the payload are shown as $\bar{E}_p$. E_T is the electron energy corrected to the top of the atmosphere. $\bar{E}_T$, $\bar{E}_p$ and ΔE_p were determined assuming a power law obtained from the observed spectrum and using the appropriate convolutions (Buffington et al. 1975). The column (Jp) represents the flux measured at float altitude. The calculation of Jp includes corrections for bremsstrahlung losses in the instrument above the spectrometer. It also includes correction for electrons produced by hadronic interactions in the atmosphere. The flux at the top of the atmosphere, J_T, was determined by finding the incident flux which, when propagated to float altitude by using the cascade theory, best matches the measured flux, Jp.

TABLE II – Summary of e^- observations.The rigidity is determined directly from the momentum spectrometer data. Ep and Jp relate to measurements at the top of the payload. E_T and J_T have been corrected to the top of the atmosphere.

Rigidity (GV/c)	N_e	$A\Omega\tau\varepsilon$ (m^2 sr s)	$\bar{E}p$ (GeV)	Jp (e^-/m^2 sr s GeV)	E_T (GeV)	$\bar{E}_T$ (GeV)	J_T (e^-/m^2 sr s GeV)
1.00					1.30		
	214	53.4	1.40	7.06 ± 0.49		1.60	6.69 ± 0.42
1.50					1.96		
	149	53.4	1.99	5.04 ± 0.41		2.27	4.86 ± 0.41
2.00					2.51		
	106	53.4	2.56	3.73 ± 0.38		2.92	3.34 ± 0.33
2.50					3.25		
	72	48.5	3.13	2.45 ± 0.29		3.57	2.26 ± 0.23
3.00					3.91		
	81	48.5	3.95	1.56 ± 0.19		4.51	1.44 ± 0.15
4.00					5.22		
	52	48.5	5.10	0.92 ± 0.12		5.82	0.77 ± 0.10
5.00					6.52		
	67	48.5	7.32	0.32 ± 0.05		8.36	0.25 ± 0.04
8.33					10.86		
	24	48.5	14.11	0.033 ± 0.004		16.11	0.026 ± 0.004
20.00					26.08		

The e^- fluxes determined in Table II along with data from previous experiments published in the last ten years are plotted in Figure 3. Data from Golden et al. (1984), were gathered in 1976, those from Tang (1984) in 1980 and those from Garcia – Munoz et al. (1988) in 1980 and 1982. The results of experiments that did not distinguish electrons and positrons have been devided by 1.1 (the measured ratio of $e^+/(e^+ + e^-)$ is about 0.1 in the energy interval 5.2 – 13 GeV (TOA)).

b) positron results:

Eighteen events passing the e^+ selection criteria were found in the interval 3–10 GV/c. Inspection of these events revealed that all had dense, forward–collimated cascades beginning in the top few layers of the calorimeter. Were protons present in the sample, roughly half of them would pass through the calorimeter without interacting, and the other half would give low multiplicity, wide angle cascades that started at various dephts in the calorimeter. Since all observed cascades appear to be electromagnetic cascades, we conclude that no proton background is present.

The $e^+/(e^+ + e^-)$ ratio is determined by selecting both positrons and electrons with the same cuts used for positrons. The selection was made in four rigidity intervals from 3 to 10 GV/c as shown in Table III. Table III also contains estimates of the atmospheric backgrounds. The numbers of atmospheric background electrons and positrons were calculated using the atmospheric spectra given by Stephens (1981).

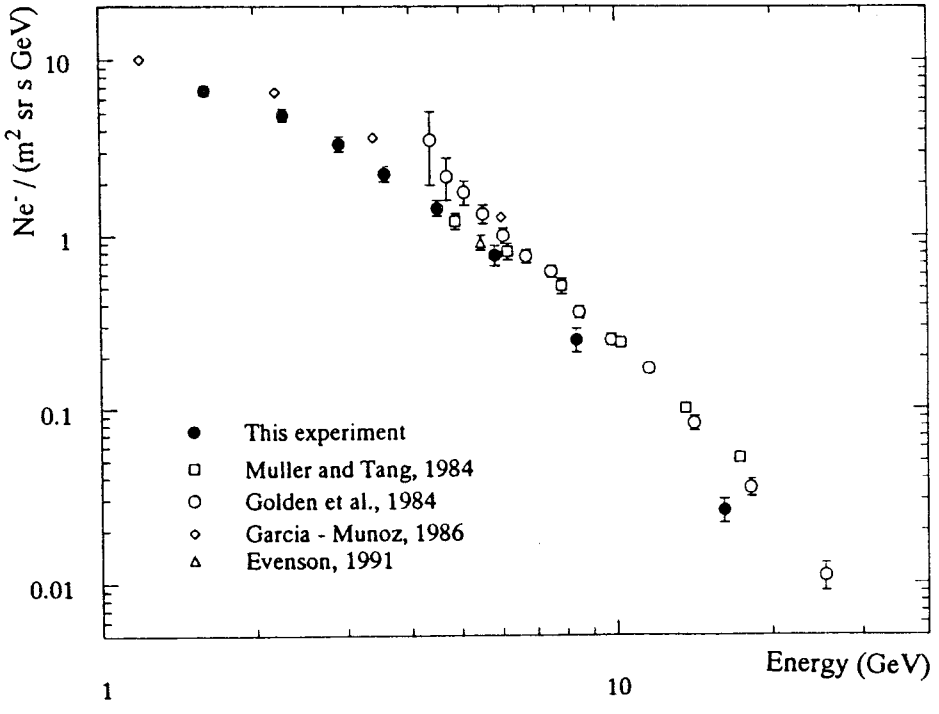

FIG. 3. A plot of the electron flux at the top of the atmosphere (from Table II). A power law spectrum to the data above 4 GeV gives $J_{e^-} = 177\ E^{-(3.15 \pm 0.13)}$ particles/(m^2 sr s GeV). For comparison, results from recent experiments are shown.

TABLE III – Subtraction of e^+ and e^- atmospheric background.

Rigidity (GV/c)	E_T (GeV)	Total number of e^-	Number of e^- with e^+ cuts	Total number of e^+	Number of e^- backgr. product.	Number of e^+ backgr. product.	Number of e^- after backgr. subtr.	Number of e^+ after backgr. subtr.
3.00	3.91							
		81	48	3	0.77	0.96	47.23	2.04 ± 1.98
4.00	5.22							
		52	38	5	0.45	0.55	37.55	4.45 ± 2.36
5.00	6.52							
		48	43	6	0.49	0.58	42.51	5.42 ± 2.57
7.00	9.12							
		28	26	4	0.27	0.31	25.73	3.69 ± 2.08
10.00	13.04							

In Table IV the e^+ flux values at the top of the atmosphere and the $e^+/(e^+ + e^-)$ ratios are given. It should be noted that in addition to background e^+ and e^- caused by nuclear interactions of cosmic rays with the atmosphere above the payload, the primary e^+ and e^- undergo cascade multiplication in the overlying atmosphere. This cascade multiplication dilutes the incident charge ratio, especially due to the large fraction of e^- in the primary radiation. We have propagated the e^+ and e^- spectra in the atmosphere to estimate this small dilution factor.

The observed fraction of e^+ is thus reduced by the factor C [Table IV] to correct for the e^+ excess produced by the electromagnetic showers of cosmic ray electrons and positrons. The data from Table IV and from some of the previous experiments are shown in Figure 4. Above 5.2 GeV (TOA) the $e^+/(e^+ + e^-)$ ratio is quite consistant with being constant. In the interval 3.9 – 5.2 GeV (TOA) the ratio may be somewhat smaller. This is consistant with the other observations shown in Figure 4. In the energy range 5.2 – 13 GeV (TOA) the ratio of $e^+/(e^+ + e^-)$ is found to be (0.11 ± 0.03). It should be noted that the lowest energy bin is based on extremely low statistics and incorporates large efficiency corrections.

TABLE IV – Computation of e^+ flux and charge ratio.

E_T (GeV)	$\bar{E}_T$ (GeV)	C	Jp (e^+/m^2 sr s GeV)	$e^+/(e^+ + e^-)$
3.91				
	4.51	1.03	0.060 ± 0.060	0.04 ± 0.04
5.22				
	5.82	1.03	0.086 ± 0.043	0.10 ± 0.05
6.52				
	7.68	1.03	0.042 ± 0.020	0.11 ± 0.05
9.12				
	10.85	1.025	0.014 ± 0.008	0.12 ±0.06
13.04				

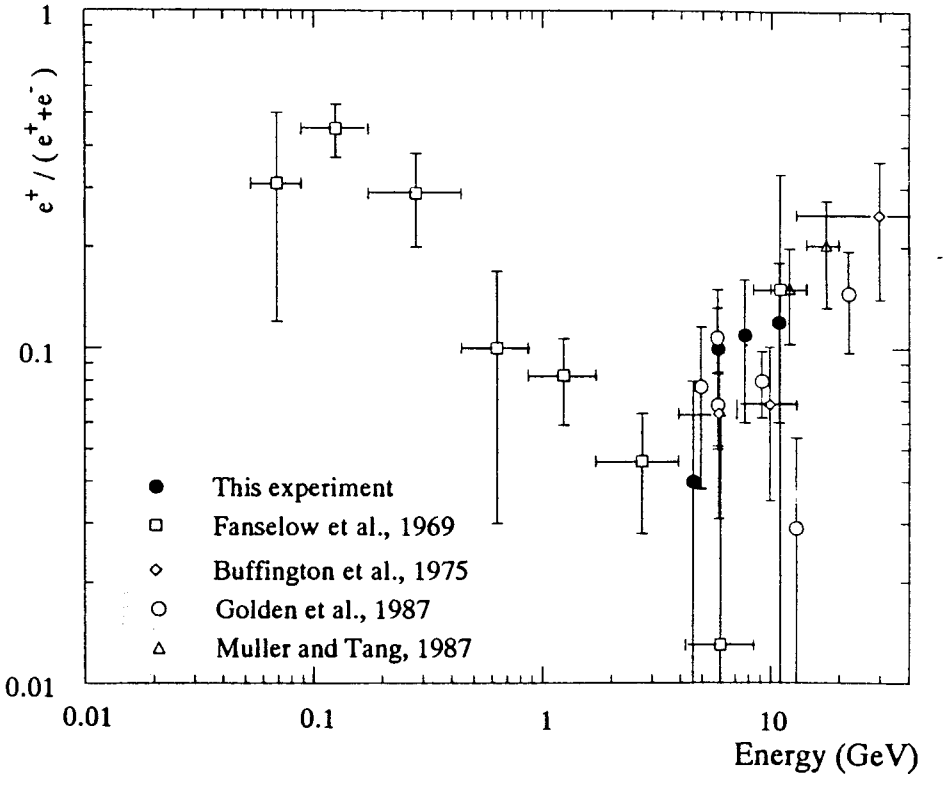

FIG. 4. – A plot of $e^+/(e^+ + e^-)$ ratio as measured in this experiment along with previous experiments is shown.

5 - DISCUSSION

5.1 – multiple cascade events:

The calorimeter images of many of the e^- and e^+ events contained multiple electromagnetic cascades. In the case of double cascades, both cascades started at (or very near) the top of the calorimeter. One cascade was aligned with the MWPC track and the other was nearby, and in the plane of the particle deflection. The showers not aligned with the MWPC track are believed to be γ–rays emitted as bremsstrahlung radiation in S1, T1, or T2. Figure 2d shows a typical multiple cascade event. Detection of accompanying γ–rays has been used in a past experiment for the identification of electrons and positrons (Buffington et al. 1975). In order to be readily recognizable, the γ–ray must have about 50 MeV of energy. At this energy, the conversion products can traverse at least 3 layers. The mean number of photons (>50 MeV) emitted by a 4 GV/c electron passing through the 0.14 g/cm^2 of material above the spectrometer is 0.72. Thus the fraction of events accompanied by γ–initiated cascades is $(1 - e^{-0.72}) = 0.51$. This is consistent with the observed fractions of e^- and e^+ multiple shower events. Buffington et al. have pointed aut that the bremsstrahlung energy losses do not change the spectral index of the electrons. The spectral index of the e^- multiple cascade events was measured as a cross–check. It was found to be identical to the overall sample. It should be pointed out that as the energy increases, the bending of the electron in the magnetic field decreases. Eventually, the γ cascade will overlap with the e^- cascade. This is expected to occur in the 20–40 GV/c range.

5.2 – Electron flux and neutron monitor data

We have determined the flux of electrons and positrons (combined) in the energy interval 5–6 GeV at the top of the atmosphere and obtained a value of 1.01 ± 0.12 electron / (m^2–sr–s–GeV). The Newark neutron monitor rate was 2952 on the day of the flight. We have plotted this flux value along with the other measurements in the same energy range in Figure 5, as a function of the date of observation (from 1970 to 1990).

The flux is plotted together with the Newark neutron monitor data. The data have been taken from the compilation by Evenson et al. (1991). It can be seen that the present result agrees well with the data from ICE experiment. The ICE flux value of 1.02 ± 0.11 electron / (m^2–sr–s–GeV) obtained on the same day as our experiment is in excellent agreement with our result. We have also obtained the flux in the same energy range from our earlier experiment (Golden et al. 1984), which was carried out on May 20, 1976 from Palestine, Texas. The value of this flux is 1.69 ± 0.17 electron / (m^2–sr–s–GeV), and the corresponding neutron monitor rate was 3256. These data points also show good agreement with the other data shown in the figure. Though the present experimental value is only 60% of the value obtained by Golden et al. (1984), it is clear from this figure that they are consistent with each other, when we consider the widely different solar activity during these two periods. Therefore, we believe that the possible systematic error of 20% assigned to the determination of the absolute spectrum in the present experiment is a very conservative estimate.

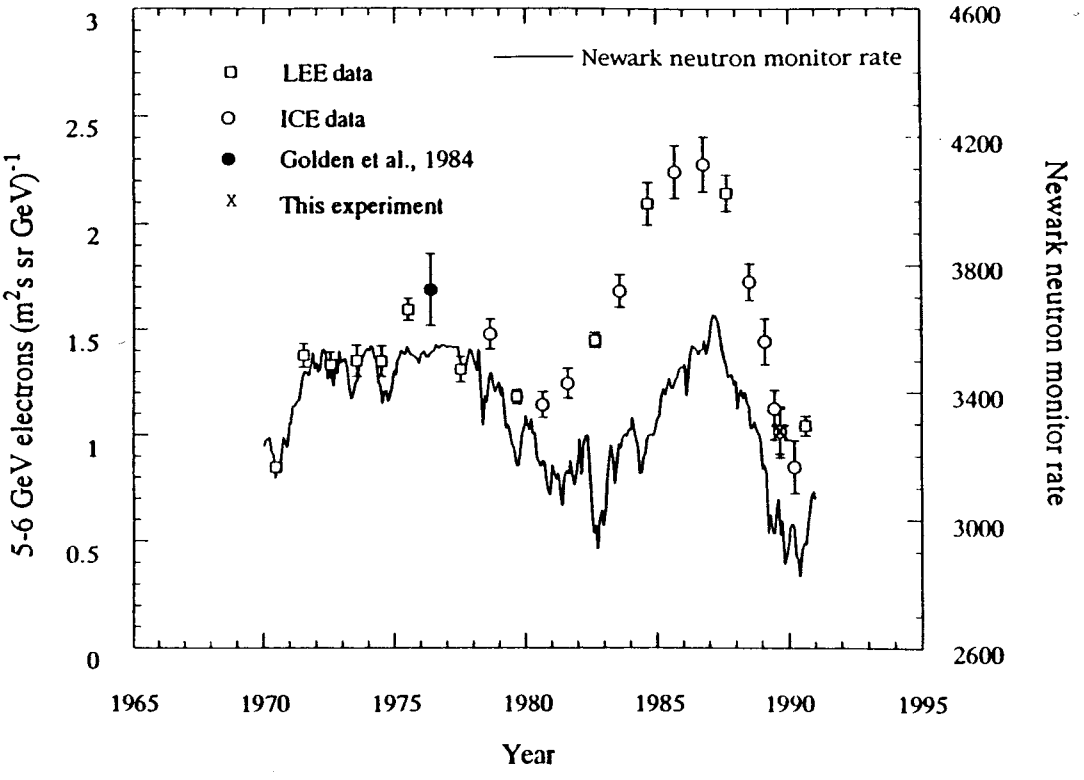

FIG. 5. Electron flux in the energy region 5 to 6 GeV (at the top of the atmosphere), is plotted with other observations and compared with the neutron monitor data. The data points represented by open symbols are taken from Evenson et al. (1991).

5.3 – Summary

Although the flight was short, it has yielded data of excellent quality. Unambiguous identification of both positrons and electrons has been accomplished. As the methods for quantitative topological separation using the calorimeter data are improved, the energy range over which separations can be performed will be increased. The $e^+/(e^+ + e^-)$ ratio is quite consistant with previous measurements in the same energy range. As mentioned earlier, the future use of a TRD detector instead of a gas Cherenkov detector should allow unambiguous e^+ observations to much higher energies than reported here.

6 – ACKNOWLEDGMENTS

This work was supported by NASA grant NAG–110, the Istituto Nazionale di Fisica Nucleare, Italy and the Agenzia Spaziale Italiana. We wish to thank National Scientific Balloon Facility and the NSBF launch crew that served at Prince Albert. Finally, we wish to give special thanks to our techical support crews from NMSU and INFN.

REFERENCES

- B. Agrinier, Y. Koechlin, B. Parlier, J. Paul, J. Vasseur, G. Boella, C. Dilworth, L. Scarsi, G. Sironi, A. Russo. 1969, *Lett. Nuovo Cimento*, ser. 1, **1**, 53.
- G. Basini, F. Bongiorno, M.T. Brunetti, A. Codino, R.L. Golden, C. Grimani, B.L. Kimbell, M. Menichelli, A. Morselli, J.F. Ormes, M.P. De Pascale, P. Picozza, M. Ricci, I. Salvatori, E.S. Seo, P. Spillantini, S.A. Stephens, R.E. Streitmatter, S.J. Stochaj, W.R. Webber. 1991, *Proc. 22nd International Cosmic Ray Conference (Dublin)*, **2**, 137.
- A. Buffington, C.D. Orth, G.F. Smooth. 1975, *Ap. J.*, **199**, 669.
- R.R. Daniel, S.A. Stephens. 1967, Proc. Indian Acad. Sci. **45A**, 319.
- P. Evenson, E. Tuska, J. Esposito, P. Meyer. 1991, *Proc. 22nd International Cosmic Ray Conference (Dublin)*, **3**, 505.
- J.L. Fanselow, R.C. Hartman, R.H. Hildebrand, P. Meyer. 1969, *Ap. J.*, **158**, 771.
- M. Garcia–Munoz, P. Meyer, K.R. Pyle, J.A. Simpson, P. Evenson. 1986, *J. Geophys. Res.*, **91**, n. A3, 2858
- R.L. Golden, S. Horan, B.G. Mauger, G.D. Badhwar, J.L. Lacy, S.A. Stephens, R.R. Daniel, J.E. Zipse. 1979, *Phis. Rev. Letters*, **43**, 1196
- R.L. Golden, B.G. Mauger, G.D. Badhwar, R.R. Daniel, J.L. Lacy, S.A. Stephens, J.E. Zipse. 1984, *Ap. J.*, **287**, 622
- R.L. Golden, S.A. Stephens, B.G. Mauger, G.D. Badhwar, R.R. Daniel, S. Horan, J.L. Lacy, J.E. Zipse. 1987, *Astr. Ap.*, **188**, 145.
- R.L. Golden, C. Grimani. R. Hull, B.L. Kimbell, R. Park, S.A. Stephens, S. Stochaj, W.R. Webber, G. Basini, E. Bonaviri, F. Massimo Brancaccio, M. Ricci, J. Ormes, E.S. Seo, R.E. Streitmatter, F. Celletti, P. Splillantini, A. Codino, M. Menichelli, I. Salvatori, F. Bongiorno, V. Bidoli, A. Buccheri, M.P. De Pascale, A. Morselli, P. Picozza. 1991, *Nucl. Inst. Meth.*, **A306**, 366.
- R.L. Golden, C. Grimani, R. Hull, B.L. Kimbell, R. Park, S.A. Stephens, S. Stochaj, W.R. Webber, G. Basini, E. Bonaviri, F. Massimo Brancaccio, M. Ricci, J. Ormes, E.S. Seo, R.E. Streitmatter, F. Celletti, P. Spillantini, A. Codino, M. Menichelli, I. Salvatori, F. Bongiorno, V. Bidoli, A. Buccheri, M.P. De Pascale, A. Morselli, P. Picozza. 1992, PAL technical note #224, available on request. To be submitted to Nucl. Instr. Meth.
- D. Muller, K.K. Tang. 1987, *Ap. J.*, **312**, 183.
- J. Nishimura. 1967, *Handbuch der Physics*, **46**, 1.
- J. Nishimura, M. Fujii, T. Taira, E. Aizu, Y. Nomura, T. Kobayashi, K. Niu, A. Nishio, R.L. Golden, T.A. Koss, J.J. Lord, R.J. Wilkes. 1981, *Proc. 17th International Cosmic Ray Conf.* (Paris), **2**, 94.
- S.A. Stephens. 1981, *Proc. 17th International Cosmic Ray Conf. (Paris)*, **4**, 282.
- K.K. Tang. 1984, *Ap. J.*, **278**, 881.